Available online at www.sciencedirect.com
SCIENCE DIRECT®
Journal of Solid State Chemistry 178 (2005) 989–997
JOURNAL OF SOLID STATE CHEMISTRY
www.elsevier.com/locate/jssc

Preparing nanometer scaled Tb-doped Y_2O_3 luminescent powders by the polyol method

M.A. Flores-Gonzalez[a], G. Ledoux[a], S. Roux[a], K. Lebbou[a], P. Perriat[b,*], O. Tillement[a]

[a]*Laboratoire de Physico-Chimie des Matériaux Luminescents, Université Claude Bernard, Lyon 1, UMR-CNRS 5620, 69622 Villeurbanne Cedex, France*

[b]*Groupe d'Etudes de Métallurgie Physique et de Physique des Matériaux, Institut National des Sciences Appliquées, UMR-CNRS 5510, 7 avenue Jean Capelle, 69621 Villeurbanne Cedex, France*

Received 18 August 2004; received in revised form 19 October 2004; accepted 21 October 2004

Abstract

Sub-micrometer Tb-doped Y_2O_3 luminescent powders were prepared from nitrate precursors using the polyol method. Just after precipitation, the powders consist of agglomerates with a spherical shape and a size ranging between 400 and 500 nm. Each agglomerate is composed of ultra-small crystallites (from 3 to 6 nm) of a bcc oxide phase whose luminescence presents original features in comparison with bulk materials. Powders were further calcinated at different temperatures and for annealing below 900 °C, highly crystalline samples with the classical green $^5D_4 \rightarrow {}^7F_5$ luminescent transitions of Tb^{3+} ions are obtained. For optimized annealing temperatures, sintering between the agglomerates is avoided and a sub-micrometric powder with a narrow size distribution and a high luminescence is obtained.

Keywords: Nanocrystals; Tb-doped Y_2O_3; Polyol method; Luminescence

1. Introduction

The remarkable properties of lanthanide ions render them extremely interesting in a large number of applications as varied as fluorescent lighting, color television, computer monitors, X-ray imaging, or amplifiers for fiber-optics communications [1–3]. Particular attention has been drawn to trivalent Tb ions ($4f^8$) as a doping element in hosts as yttrium or gadolinium oxide because of its narrow green bands originating from intra 4*f*-transitions. Under excitation at 280 nm it presents a series of emissions ranging from 460 to 700 nm relative to the transitions between the $^5D_4$ and ^7F_n ($n = 0$–6) levels [4,5]. In a number of applications, the phosphors used are powders of large particles with a size ranging between 5 and 20 μm obtained from a conventional ceramic route involving high-temperature solid-state reactions [6,7]. However, in order to facilitate the deposition by spraying of the powder and also to increase the resolution of optical devices, there is a clear need for decreasing the particles size of the powder. In conventional processes, the size reduction can be achieved only by comminution techniques which results in a corresponding reduction of luminescence efficiency ascribed to the formation of a large amount of bulk defects [8]. Other synthesis routes are then required for obtaining sub-micrometer sized particles free of these defects. Numerous methods were already reported to prepare rare-earth-doped yttrium oxide with a high surface area: liquid phase methods [9,10], self-burning and glycine-assisted combustion methods [11–13], most of them being based on a sol–gel process [4,14,15]. They lead to nanometer-sized particles with a luminescence efficiency strongly reduced compared to that of macroscopic samples [16]. This is due to the strong

*Corresponding author. Fax: +33 4 72 43 85 28.
E-mail address: pascal.perriat@insa-lyon.fr (P. Perriat).

0022-4596/$ - see front matter © 2004 Elsevier Inc. All rights reserved.
doi:10.1016/j.jssc.2004.10.029

contribution of a surface dead layer which facilitates non-radiative recombination routes. The most attractive possibility for obtaining sub-micrometer powders with satisfying optical properties consist then in preparing nanometric particles by a soft chemistry route and then increasing their size by some appropriate thermal annealing. We have already shown that this could be processed by synthesizing the powders using a sol-lyophilization technique, the hydroxide powders obtained being further converted into the adequate oxide phase by calcinations at moderate temperature ($<900\,^{\circ}C$) [17]. In this paper we will evidence that it is also possible to prepare sub-micronic Tb-doped Y_2O_3 particles by the polyol method.

The polyol method is based on the direct precipitation in a high boiling alcohol, here the diethylene glycol (DEG). It has been successfully used to prepare a large variety of materials including oxides [18–20], sulfides [21], phosphates [22] and elemental metals [23,24]. It allows an almost perfect control of the particle size because the alcohol acts as a surface capping agent [25]. In the case of rare-earth-based oxides, the nature of the precursor is crucial for determining the state of agglomeration of the particles formed. When starting from chlorides, some colloidal solutions stable for months are prepared [16]. However when starting from nitrates, suspensions of sub-micrometric agglomerates (0.1–1 μm) each of them composed of nanometric particles (3–5 nm) are obtained. The size of the agglomerates can be adjusted by varying some synthesis parameters such as the temperature or the concentration of the cations introduced. This is then very suitable for preparing sub-micrometric powders: after filtration the only difficulty consists in finding the adequate annealing for eliminating the residual DEG, densifying the agglomerates and improving the optical properties by a size increase of the elemental particles. Avoiding any coalescence of the agglomerates during the annealing is a key point for obtaining a powder with a narrow size distribution which is a stringent requirement for device applications. It is then the main objective of the present paper to determine the optimized conditions for a complete intra-agglomerates sintering (between the particles within the agglomerates) without any concomitant inter-agglomerates sintering (between the agglomerates of the powder). Studying in the same time the growth of the particles and the correlative evolution of the luminescence intensity is also crucial for determining the most suitable parameters for annealing. This will provide interesting information about the influence of the grain size upon the optical properties which is a subject very rarely treated in the case of rare-earth oxides due to the difficulties of synthesizing model samples differing only by the grain size.

2. Experimental

2.1. Synthesis

Stoichiometric mixtures of $Y(NO_3)_3$ and $Tb(NO_3)_3$ 99.99% solutions (nitrate salts were kindly provided by the Rhodia Electronics & Catalysis Company, France) were dispersed in 100 mL of DEG (99%, *Aldrich*) with a global metal concentration of 0.1–0.5 mol L^{-1}. After intensive stirring, 2 mL of demineralized water was added and the mixture heated in a silicon oil bath to 140 °C. The whole mixture was heated for 1 h, the components were dissolved and the liquid became clear. Then the solution was mixed by vigorous stirring for 4 h in refluxing diethylene glycol at 180 °C and, as a result, a suspension is obtained. In the case where NaOH was also added at 140 °C, hydroxides were formed exactly as they do during hydrothermal synthesis performed at high pH [26,27]. However, when no NaOH was added, oxides were the only phases obtained. In this latter case, a suspension of sub-micrometer agglomerates (≈few hundreds of nanometers) composed of nanometric particles (≈few nanometers) was obtained. The formation of oxide occurs according to the following reaction:

$$2M(NO_3)_3 + 3H_2O \rightarrow M_2O_3 + 6HNO_3,$$

where *M* denotes either Y or Tb.

At the end of the annealing, water was completely removed in order to avoid further transformation to hydroxide of the oxide formed. The size of the agglomerates can be varied in a broad range going from 20 nm to 1 μm by adjusting parameters such as the concentration of the rare-earth cations, the temperature, the duration of the annealing, the quantity of water introduced. The agglomerates studied here have a size of around 400 nm; they can be then easily separated from the solvent by precipitation and filtration through 0.22 μm sieves. The white precipitate was later washed with methanol and then dried in a stove at 100 °C for 1 h. The powder was subsequently thermally heat treated at different temperatures, 300, 500, 700 and 900 °C with a programmed heating rate of 10 °C min^{-1} for 3 h in a weakly reducing atmosphere consisting of a hydrogen–argon mixture containing 5 vol% of H_2. Annealing under reducing conditions is necessary to avoid the oxidation of the Tb cations to the non-luminescent Tb^{4+} cation which would occur under room atmosphere.

The reaction yield is almost 100%. It is significantly higher than that obtained when starting from chlorides which is around 30%. It is then possible to avoid the operation of dialysis indispensable to achieve the purification of the colloids obtained with the use of chlorides.

2.2. Characterization

Direct measurements of the size distribution of the aggregates suspended in the polyol medium were obtained by Photon Correlation Spectroscopy (PCS) using a Zetasizer 3000 HS. For all samples, the crystalline structures of the powders were characterized by X-ray powder diffraction (XRD) using a SIEMENS D-5000 diffractometer with the Cu$K\alpha_1$ ($\lambda = 0.15406$ nm) and Cu$K\alpha_2$ X-rays ($\lambda = 0.15444$ nm). The diffraction pattern was scanned over the 2θ range 15–70° in steps of 0.06° and a counting time of 6 s/step. The parameter of the crystalline sample has been refined taking into account the aberration arising from the specimen displacement, $D_{2\theta}$, given by the formula: $D_{2\theta} = -2s/R \cos 2\theta$ where s is the displacement of the sample surface with respect to the axis of the goniometer and R the radius of the goniometer circle. The microstrains and the size of the coherent domains have been derived from a refinement of the full-width at half-maximum (FWHM), β, of the patterns fitted with pseudo-Voigt functions according to the following relation: $\beta^2 = U \tan^2\theta + \mathrm{IG}/\cos^2\theta$. In the latter relation U is an estimate of the isotropic broadening due to the presence of microstrains: $\varepsilon = \pi/1.8\sqrt{U}$ (ε the defect concentration in %) and IG is a measure of the isotropic size effect: $T = 180K\lambda/\pi\sqrt{\mathrm{IG}}$ (T the size in Å, λ the wavelength in Å and K the Scherrer constant here equal to 4/3) [28]. The FWHMs have been corrected from the instrumental corrections obtained from an annealed BaF_2 reference.

High-resolution transmission electronic microscopy (TEM) was performed using a JEOL 2010 microscope operating at an accelerating voltage of 200 kV (resolution of 1.5 Å). Specimens were prepared by diluting in methanol some agglomerates milled in order to disperse some of the particles forming the agglomerates; then a drop of the dilution was placed on a holey carbon support film carried by a copper grid and dried. For scanning electron microscopy (SEM) a Hitachi S-800 apparatus equipped with a LaB6 cathode was used. The samples were sputtered with gold.

Thermogravimetric analysis experiments (TGA) have been perfomed in a SETARAM Tag 24 balance upon ≈20 mg of powder. Successive heating up to 1200 °C and cooling have been made at a rate of 2 °C min^{-1} either under a flow of pure oxygen or a mixture of hydrogen (5 vol%)/argon (95%).

Optical spectra were obtained using a 450 W Xe-lamp as the excitation source. For emission spectra, excitation was adjusted at 280 nm with a Jobin Yvon H10D monochromator. Light was then collected by an optical fiber and analyzed by a Jobin Yvon TRIAX 320 monochromator. Two resolutions were used (1200 grooves mm^{-1} grating blazed at 330 nm which ensures a resolution of 0.25 nm and 300 grooves mm^{-1} blazed at 250 nm which gives a resolution of 1.0 nm). For excitation spectra, the wavelength was selected using a Jobin Yvon H10D monochromator with a 1200 grooves mm^{-1} grating and 0.25 mm slits for both entrances giving 1 nm resolution. All experiments were carried out at room temperature.

3. Results and discussion

3.1. Structure and morphology of the sample obtained after precipitation

SEM observations show that the powder obtained after precipitation consists of large aggregates (>10 μm) composed of spherical grains with a size of around 400 nm (Fig. 1a). Dynamic light experiments show that, after dilution of the powder in DEG, the suspension presents a narrow size distribution centered at 407 nm (Fig. 1a). That means that the grains in the aggregates

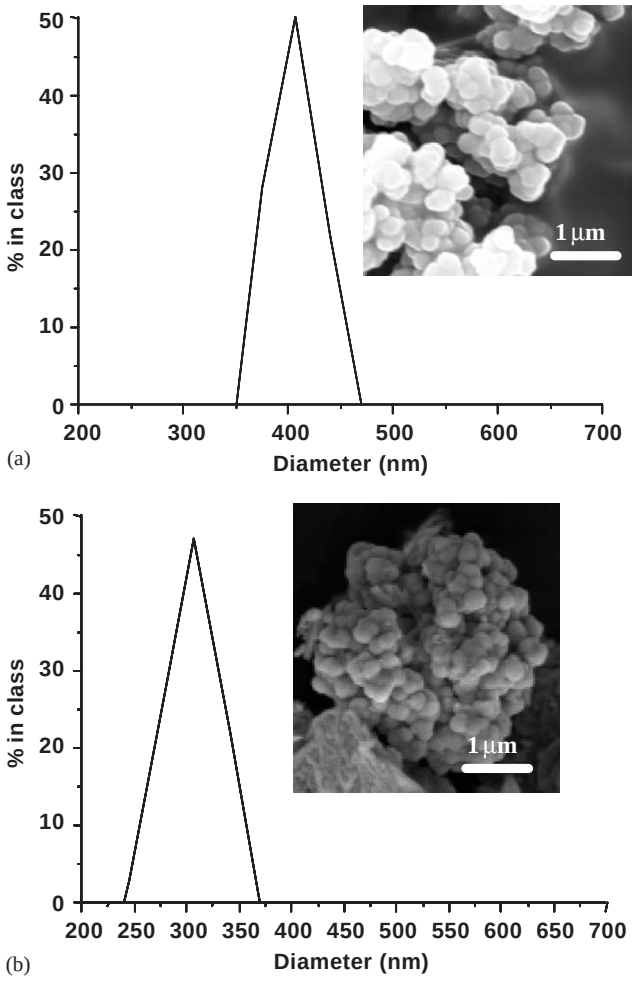

Fig. 1. Size distribution obtained by laser measurements and in inset SEM image of a 5% Tb-doped Y_2O_3 powder just after precipitation (a) and after annealing at 700 °C (b).

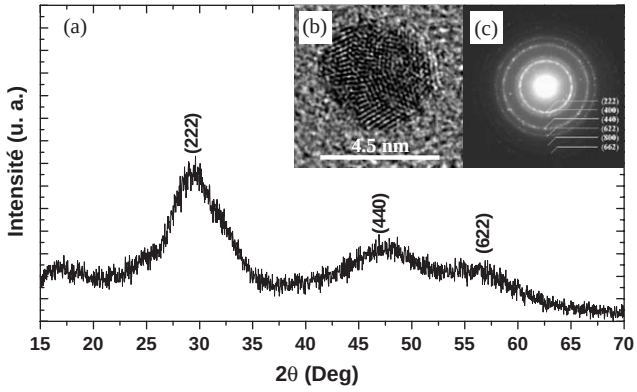

Fig. 2. (a) X-ray diffraction diagram of a 5% Tb-doped Y_2O_3 powder obtained after synthesis, (b) high-resolution TEM micrograph of the particles constituting the agglomerates with visualization of the (222) planes and (c) electron diffraction patterns of fragments of agglomerates.

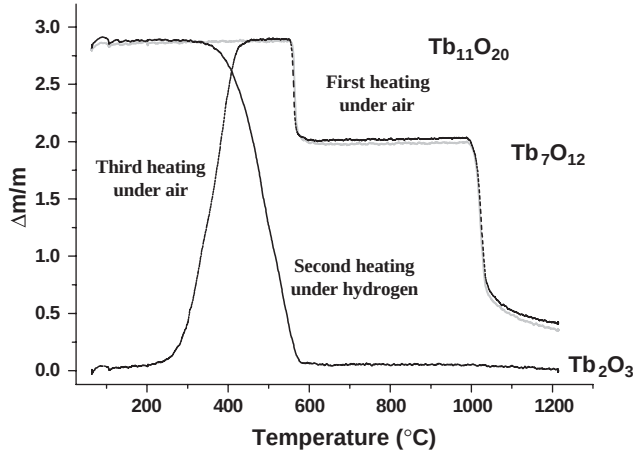

Fig. 3. Thermogravimetric analysis for a pure terbium oxide powder subjected to three heating/cooling cycling at a rate of 2 °C min^{-1} under air for the first heating (solid gray line), under a mixture of hydrogen and argon for the second (solid black line), under air for the last (dashed line).

can be easily re-dispersed and then gather in the aggregates only by weak interactions. Each grain ($\approx$400 nm) is itself an agglomerate: it is composed of nanoparticles with a size lying between 4 and 5 nm. These particles can be evidenced by TEM observations since after milling of the powder, dilution in ethanol and deposition on a grid, a few of them are lying alone. These particles, assumed to be representative of those remaining in the fragments of the agglomerates, are evidenced in the inset of Fig. 2b. They are polycrystalline with a crystallite size of around 3 nm.

The powder obtained just after synthesis is crystalline as inferred from the (222) planes visible on the MET micrograph, the electron diffraction patterns recorded on some fragments of the grains and the X-ray diffraction diagram recorded on the powder (Fig. 2c). The patterns of both diagrams are consistent with the usual bcc structure of yttrium oxide (space group $Ia\bar{3}$, No. 206 in the ITC numeration). A significant part of the scattered intensity belongs to the diffraction peaks which confirm the crystallization of the powder already evidenced by TEM. Also consistent with the crystallite size measured by TEM (3 nm) is the size of the coherent domains deduced from the width at half maximum of the X-ray diffraction patterns (3 nm). Although well crystallized, the particles present some strong structural disorder as planes curvature or lack of atom columns.

3.2. Determination of the atmosphere conditions for thermal annealing

We already mentioned the necessity of thermal annealing for elimination of the alcohol and optimization of the optical properties. For annealing under air below 1000 °C, Y_2O_3 is chemically stable with a valence 3 for yttrium. On the contrary, Tb undergoes some valence change between Tb^{3+} and Tb^{4+}. It is then essential to control the oxygen partial pressure (pO_2) for obtaining only Tb^{3+} which is the cation interesting for luminescence. This has been made by performing the annealing in reducing conditions under a mixture of hydrogen and argon. Such atmosphere conditions have been validated by studying the Tb oxido-reduction reactions by TGA. Fig. 3 exhibits the mass change of a reference sample subjected to three successive thermal cycling under either oxidizing or reducing atmospheres (for clarity only heating is shown). The reference sample consists of a powder of pure Tb oxide prepared by the precipitation method described here and annealed at 1200 °C under air for elimination of organic residues. It has been cooled slowly to obtain the valence stable in room conditions, i.e., 3.64 ($Tb^{3.64+}$) corresponding to the mean valence of Tb in $Tb_{11}O_{20}$ [29]. The three successive cycling consist of a heating at a rate of 2 °C min^{-1} up to 1200 °C followed by a cooling at the same rate. They are performed under air for the first annealing, a mixture of hydrogen and argon for the second and air again for the third. The mass changes observed in Fig. 3 show that the first heating under air presents different reduction steps which can be assigned to the transformation of $Tb_{11}O_{20}$ to Tb_7O_{12} at $\approx$600 °C (an exp. mass change of 0.90% for an expected one of 0.88%) and that of Tb_7O_{12} to Tb_2O_3 after 1000 °C (an exp. mass change of 1.84% for an expected one of 1.82%). The variations of the oxygen stoichiometry during the transformations are sharper than those reported in samples obtained by classical solid-state reactions [30] probably because of the nanometric structure of the sample (crystallite size $\approx$80 nm after annealing at 1200 °C) which fastens the diffusion mechanisms. When cooling under air, Tb re-oxidizes

up to $Tb^{3.64+}$ and during the second annealing which is made under hydrogen, the reduction processes in only one step leading directly to Tb_2O_3 below 600 °C. When cooling in the same reducing atmosphere, there is no more change of the Tb^{3+} valence and for the last heating under oxygen, further Tb oxidation only occurs around 300 °C. It oxidizes to the valence which is thermodynamically stable ($Tb^{3.64+}$) as soon as the diffusion processes become fast enough. The oxidation is then followed by the reduction already observed for the first annealing. In this paper, Tb-doped Y_2O_3 is obtained by annealing the precipitates obtained by the polyol method (and only containing Tb and Y at the valence 3) under reducing atmospheres. All the results obtained by TGA show then that the mineral part of the powder has always the composition Tb_2O_3 whatever the temperature chosen for annealing.

3.3. Evolution of the structure and the morphology of the samples during annealing in reducing atmosphere

The evolution with annealing of the structure and of the morphology of the agglomerates has been followed by X-ray diffraction (Fig. 4). For annealing at 300 °C, the peaks are still considerably broadened. The contribution of the defects to the FWHM is small compared to that of the size; then only the crystallite size can be obtained from the pattern broadening. For a Tb content of 5%, it is equal to 6 nm (Table 1) which corresponds well to the size of the particles constituting the agglomerates. This indicates that a transition from a polycristalline to a monocrystalline state occurs within the elemental particles below 300 °C. It is confirmed by the high-resolution TEM image of Fig. 5 where the (222) planes of the bcc phase are seen to cross continuously

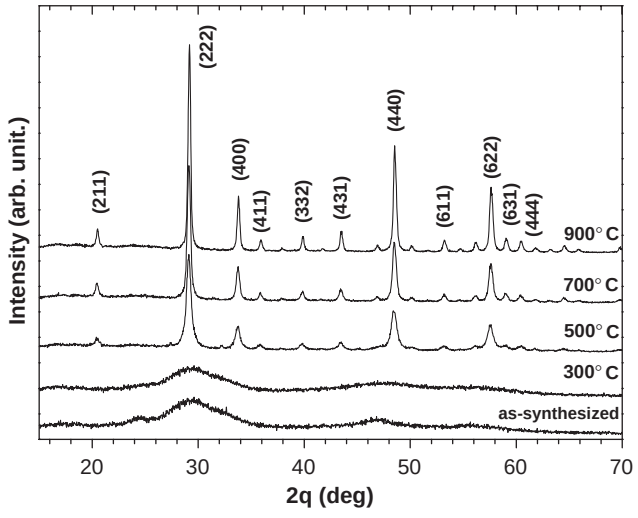

Fig. 4. X-ray diffraction patterns of 5% Tb^{3+}-doped Y_2O_3 powders as-synthesized and annealed for 2 h under a mixture of hydrogen/argon at different temperatures comprised between 300 and 900 °C.

the entire particle annealed at 300 °C. The image also shows that some structural disorder still remains after annealing at 300 °C.

With increasing the annealing temperature the diffraction patterns become progressively narrower which corresponds to a simultaneous increase of the crystallite size and to a decrease of the defect content. Size and defect content are given in Table 1 for the sample doped with 5% Tb. Above 700 °C, the defect content is very small which indicates that the state of crystallization of this sample is almost perfect. Fig. 6 shows the evolution of the lattice parameter as a function of the Tb^{3+} concentration for the samples annealed at 500, 700 and 900 °C. It does not depend on the annealing temperature which indicates the absence of chemical impurities such as hydroxyl groups within the crystal (their release during annealing should have been accompanied by some change of the parameter). There is also a perfect agreement between the composition dependence of the parameter found experimentally and a theoretical fit assuming that the Y_2O_3–Tb_2O_3 solid solution follows the Weggard's law. In such a fit, the values of the lattice parameters of Y_2O_3 and Tb_2O_3 were adjusted to respectively 10.6015 Å and 10.7195 Å which are values very close to those given by the JCPDS files: 10.60 Å for Y_2O_3 (File No. 41-1105), 10.73 Å for Tb_2O_3 (File No. 23-1418). A solid solution between yttrium and terbium oxides is then obtained whatever their relative concentration which is easily explained by the fact that both crystallize in the same bcc phase and have similar values of atomic radii.

The morphology of the agglomerates was also followed by laser measurements with the aim to characterize their intra- and inter-sintering. Intra-sintering can be evidenced by a size decrease of the agglomerates, inter-sintering by an increase. For this purpose, the powders annealed were re-dispersed in three different solvents, DEG, water and ethanol by ultra sonication for 15 min. At 300 °C, DEG was not removed completely and the organic residues act as a "glue" which avoids a complete re-dispersion of the agglomerates. It is only for the samples annealed above 500 °C that DEG is completely eliminated and photon correlation spectroscopy can provide some relevant information upon the size of the agglomerates. Compared with their initial size of 407 nm, a size decrease to 315 nm is observed after annealing at 500 °C and to 306 nm at 700 °C. It indicates a densification of each agglomerate related to the disappearance of the porosity let by the removing DEG. This densification of 56% corresponds almost exactly to the volume occupied by the DEG contained in the agglomerate just after precipitation. This latter has been indeed evaluated to 52% from thermogravimetric analysis. That the complete densification of the agglomerates is achieved as soon as 500 °C is confirmed by the fact that the

Table 1
Morphology of a 5% Tb-doped Y_2O_3 powder

Annealing temperature (°C)	As synthesized	300	500	700	900
Crystallite size (nm)	3±0.5	6±1	21±2	35±3	58±10
Defect content (%)			1.0±0.1	0.35±0.05	0.26±0.05
Agglomerate size after dispersion (nm)					
In DEG	407 (11)	690 (22)	315 (16)	306 (15)	520 (57)
In ethanol	390 (16)	650 (20)	310 (20)	320 (16)	520 (62)
In water	400 (14)	650 (21)	300 (18)	320 (17)	500 (55)

For characterizing the crystallites are given the average size and the defect content (for annealing at low temperatures, only the size contribution to the pattern broadening is taken into account). For characterizing the agglomerates are given the average size and, in parenthesis, the mean standard deviation.

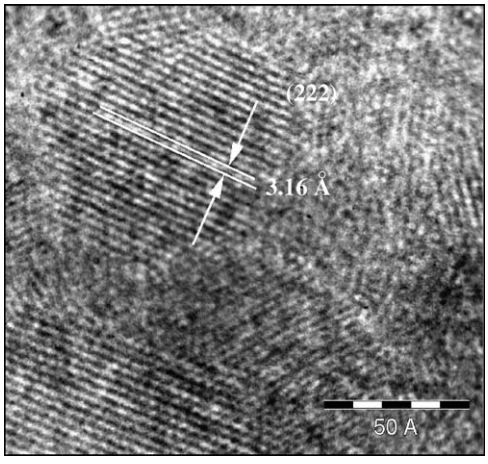

Fig. 5. High-resolution TEM micrograph of the particles constituting the agglomerates after calcination at 300 °C. Visualization of structural defects.

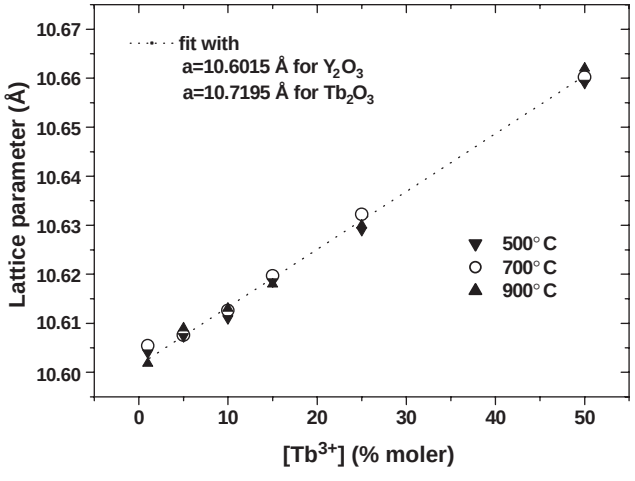

Fig. 6. Evolution of the lattice parameter with terbium concentration after annealing at 500, 700, 900 °C under a mixture of hydrogen/argon.

agglomerates size does not decrease significantly more with annealing at higher temperatures. Fig. 1b shows the size distribution obtained by photon correlation spectroscopy and the SEM image of the agglomerates annealed

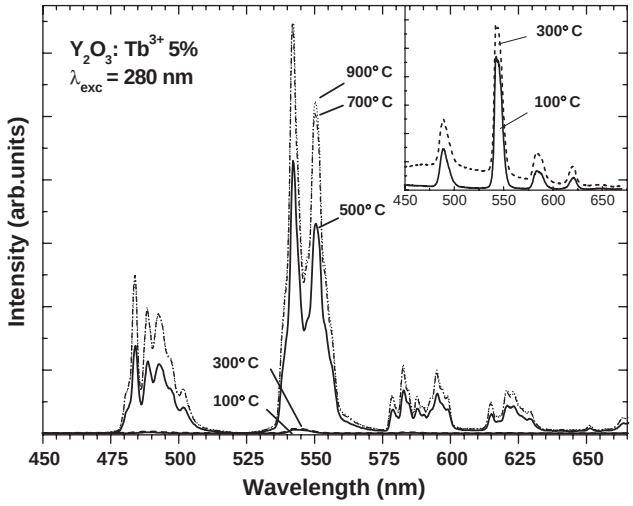

Fig. 7. Room temperature luminescence spectra of Y_20_3:Tb^{3+} (5%) powders just after synthesis and after annealing at different temperatures between 300 and 900 °C.

at 700 °C. Except that the average size has visibly diminished they present exactly the same characteristics than the powder obtained after precipitation: a narrow distribution hardly widened and an always clear separation between the agglomerates. Inter sintering between the agglomerates is evidenced only at 900 °C by a slight increase of the agglomerate size. It is therefore possible not only to remove completely the residual DEG but also to achieve a full densification of each agglomerate, avoiding any aggregation between them. For this the annealing temperature must be comprised in a large range around 500–700 °C. As seen in Table 1 the agglomerates obtained can be further re-dispersed in a large variety of solvents.

3.4. Effect of the thermal annealing upon the luminescence: determination of the optimal annealing

Fig. 7 shows that the luminescence of the Tb-doped sample (5%) strongly increases with the annealing temperature. In this figure the luminescence was

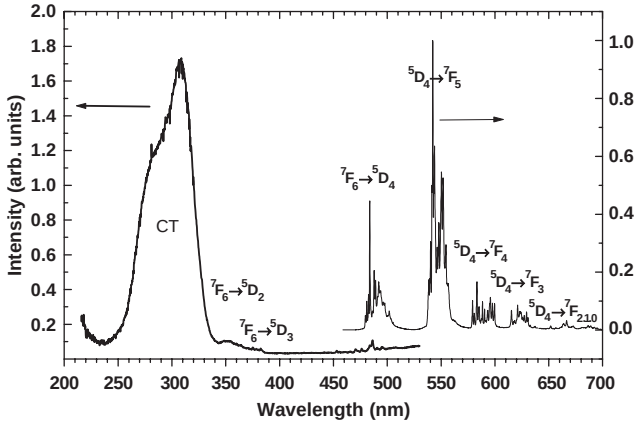

Fig. 8. Excitation and emission spectra of the optimal Tb^{3+}-doped Y_2O_3 powder (annealing temperature: 700 °C, Tb concentration: 5%).

recorded at low resolution to render more visible the comparison between the different annealing. For calcinations at temperatures lower than 500 °C, the presence of strongly absorbent organic residues decreases the luminescence intensity. However some luminescence is still observed which is an additional proof that the Tb activators are effectively inserted within a crystal just after precipitation. Indeed, the transitions between the energy levels of the rare earth are electric dipole forbidden and only the presence of a crystal field can provide a finite transition probability by mixing opposite parity configurations [31]. For the localized Tb impurities embedded in the yttrium oxide host, the effect of quantum confinement is quite different from that observed in the case of semi-conductors and the wavelength of the activator emission is essentially insensitive to the particle size. That explains why for all temperatures large emission bands between 450 and 700 nm resulting from the $^5D_4$ to ^7F_n transitions ($n=0$–6) are observed on top of a large continuum of emission (see Fig. 8 for complete indexation). However, two main characteristics can be noticed for the particles with the lower sizes (inset of Fig. 7). The first characteristic concerns the absence of any fine structure in the different transitions even when measured at high resolution. This feature probably related to some broadening of the peaks was already observed in the case of colloids of pure Tb_2O_3 [4] or with Eu^{3+} as the activator in a gadolinium oxide matrix [16]. It may be related to some perturbation of the crystal field rising from a site symmetry within the nanoparticles much less defined than in macroscopic samples. The second main characteristic of the powders with the lower particle size concerns the absence of a surface peak in the emission band. Such a peak shifted by 1 nm compared with the usual bulk one was observed in particles prepared by thermal decomposition of hydroxide [17,32,33]. The absence of this peak can be ascribed to the adsorption at the surface of a large amount of OH groups which are known to quench efficiently the luminescence [34]. These hydroxyl groups are related either to some remaining alcohol or to some physisorbed water. They have a significant influence here due to the particular interface of the particles which is either of a solid/liquid type before DEG degradation or of a solid/gas one after. The situation was quite different for the particles prepared by hydroxide decomposition in which the interface was of a solid/solid type. Any quenching related to hydroxyl adsorption was then impossible and the perturbed luminescence arising from the symmetry change at the surface could be effectively observed.

Above 500 °C the spectra become much more structured, each transition being splitted into several fine peaks corresponding to the level of degeneracy of the transition. Anyway, after 700 °C the luminescence does not increase anymore as proved by Fig. 7 which shows that the spectra at 700 and 900 °C are almost perfectly superimposed. This result was in fact expected from the structural study of the samples which showed that above 700 °C the samples were very well crystallized with a small and quasi-identical defect content. The crystallite size was also superior to 30 nm which is a range where the surface effects can be neglected [33] and the agglomerates are completely dense without internal solid/gas interface which is the main reason for surface quenching.

With the objective of determining the more appropriate annealing for obtaining a highly luminescent powder with a narrow size distribution in the submicrometric range, the temperature of 700 °C appears to be the best compromise. 700 °C indeed is the temperature where a full intra-agglomerate sintering can take place and lead to optimal optical properties but without any inter-agglomerate sintering which increases the mean agglomerate size and strongly broadens the size distribution (Table 1). Emission and excitation spectra were recorded with a high resolution (Fig. 8) for a complete characterization of the optimal sample: 5% Tb-doped Y_2O_3 annealed at 700 °C. The excitation spectrum monitored at 550 nm (the $^5D_4$–$^7F_5$ transition) clearly shows a double charge transfer band (noted CT in the figure) between 250 and 320 nm. The structured CT band shows a maximum for an excitation wavelength around 308 nm and should be assigned to a charge transfer from 2*p* orbital of oxygen to 4*f* orbital of Tb^{3+}. At the foot of this band a series of lines corresponding to transitions between the ground $^7F_6$ level and $^5D_2$ and $^5D_3$ excited levels are apparent. Finally another set of narrow bands attributed to the transition between $^7F_6$ and $^5D_4$ levels lie in the range 480–510 nm. The emission spectra presented was obtained by exciting at 280 nm in the CT bands. The emission bands have already been indexed. The noticeable fact is that the bands relative to the optimal sample

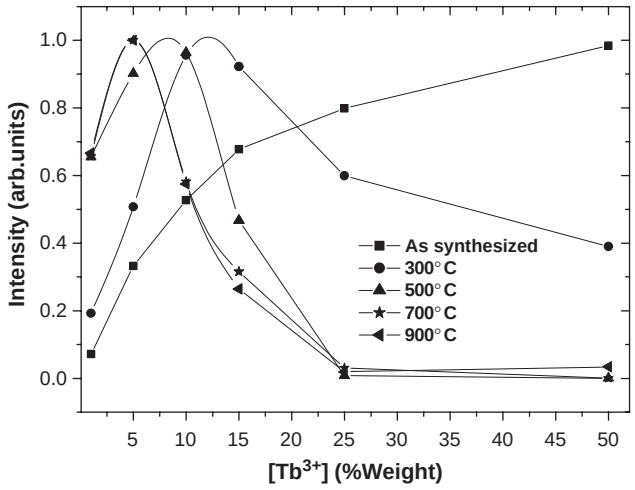

Fig. 9. Evolution of luminescence with Tb concentration for samples with different crystallite sizes varying between 3 and 58 nm.

are exceptionally well defined even compared with reference samples such as YBO_3: Tb^{3+}. The reason is probably that, with the synthesis method presented here, a full-crystallized sample can be obtained at low temperature ($<900\,^{\circ}C$) that is to say by avoiding the entropy-related defects usually generated by annealing at higher temperatures. This interpretation is rendered stronger since an annealing at 1100 °C has been verified to decrease by around 40% the luminescence intensity obtained at 700 °C. It is also consistent with the observation that the defects generated by comminution lead to the same trend.

3.5. A grain size/optical properties relationship

Fig. 9 presents the evolution of the integrated emitted band at 550 nm as a function of the Tb^{3+} ions concentration for annealing at different temperatures. Since for annealing at a given temperature, the size measured by X-ray diffraction does not depend on the Tb concentration, the evolutions reported in the figure concern in fact samples with different crystallite sizes. It is noteworthy that the maximum of luminescence of each curve strongly depends on this size. The maximum is even not visible for the sample with the lower size (3 nm) and its position decreases when the crystallite size increases. For samples with a crystallite size greater than 35 nm, the maximum does not decrease more and corresponds to that usually observed in bulk materials (between 5% and 6%). Above this critical concentration, quenching occurs due to energy transfers between the adjacent emitter ions. For the samples with the lower size, the present results indicate then that energy transfers should be prevented by the important structural disorder evidenced on TEM micrographs. This result is similar to that already observed in the case of Eu-doped YVO_4 colloids [35].

3.6. Conclusion

Re-dispersible sub-micrometric powders of Tb-doped Y_2O_3 have been prepared using the polyol method followed by reducing annealing at temperatures lower than 900 °C. Highly crystalline samples, free of the entropy-related defects generated by the classical solid reactions routes, are obtained. They are highly luminescent and present the same general features than the samples elaborated at high temperatures. An optimal value of $\approx 5\%$ has been determined for Tb doping concentration. Also an optimal temperature of 700 °C has been determined for annealing. This temperature is in the range which both permits some efficient intra-agglomerates sintering and avoids any inter-agglomerates one.

For crystallite sizes lower than 35 nm, some surface effects are noticeable upon the optical properties. Luminescence is decreased due to the quenching by a surface dead-layer and the quenching concentration is strongly increased due to some structural disorder which prevents energy transfer.

Acknowledgment

The authors are grateful to CONACyT-SFERE Program 2001 for M.A. F.-G. Mexican scholarship.

References

[1] C.R. Ronda, J. Alloys Compds 225 (1995) 534–538.
[2] G. Blasse, Chem. Mater. 1 (1989) 294–301.
[3] P. Maestro, D. Huguenin, J. Alloys Compds. 225 (1995) 520–528.
[4] G. Wakefield, H.A. Keron, P.J. Dobson, J.L. Hutchison, J. Phys. Chem. Solids 60 (1999) 503–508.
[5] R.N. Bhargava, J. Lumin. 70 (1996) 85–94.
[6] F.S. Kao, T.M. Chen, J. Lumin. 96 (2002) 261–267.
[7] S. Erdei, R. Roy, G. Harshe, H. Juwhari, D. Agrawal, F.W. Ainger, D. Agrawal, Mater. Res. Bull. 30–6 (1995) 745–753.
[8] N. Guigue-Millot, S. Bégin-Colin, Y. Champion, M.J. Hÿtch, G. Le Caër, P. Perriat, J. Solid State Chem. 170 (2003) 30–38.
[9] B.M. Tissue, Chem. Mater. 10 (1998) 2837–2845.
[10] M. Haase, K. Riwotzki, H. Meyssamy, A. Kornowski, J. Alloys Compds. 303–304 (2000) 191–197.
[11] L. Sun, J. Yao, Ch. Liu, Ch. Liao, Ch. Yan, J. Lumin. 87–90 (2000) 447–450.
[12] W.W. Zhang, W.P. Zhang, P.B. Xie, M. Yin, H.T. Chen, L. Jing, Y.S. Zhang, L.R. Lou, S.D. Xia, J. Colloid Interface Sci. 262 (2003) 588–593.
[13] G. Tessari, M. Bettinelli, A. Speghini, D. Ajo, G. Pozza, L.E. Depero, B. Allieri, L. Sangaletti, Appl. Surf. Sci. 144–145 (1999) 686–689.
[14] Y.L. Soo, S.W. Huang, Z.H. Ming, H. Kao, G.C. Smith, E. Goldburt, R. Hodel, B. Kulkarni, J.V.D. Veliadis, R.N. Bhargava, J. Appl. Phys. 83 (10) (1998) 5404–5409.
[15] Y. Tao, G. Zhao, X. Ju, X. Shao, W. Zhang, S. Xia, Mater. Lett. 28 (1996) 137–140.

[16] R. Bazzi, M.A. Flores, C. Louis, K. Lebbou, W. Zhang, C. Dujardin, S. Roux, B. Mercier, G. Ledoux, E. Bernstein, P. Perriat, O. Tillement, J. Colloid Interface Sci. 273 (2004) 191–197.
[17] C. Louis, R. Bazzi, M.A. Flores, W. Zheng, K. Lebbou, O. Tillement, B. Mercier, C. Dujardin, P. Perriat, J. Solid State Chem. 173 (2003) 335–341.
[18] L. Poul, S. Ammar, N. Jouini, F. Fiévet, F. Villain, Solid State Sci. 3 (2001) 31.
[19] C. Feldmann, Scripta Materialia 44 (2001) 2193–2196.
[20] J. Merikhi, H.O. Jungk, C. Feldman, J. Mater. Chem. 10 (2000) 1311–1314.
[21] C. Feldmann, C. Metzmacher, J. Mater. Chem. 11 (2001) 2603.
[22] C. Feldmann, Adv. Funct. Mater. 13 (2003) 101.
[23] F. Fievet, Surfactant Sci. Ser. 92 (2000) 460.
[24] G. Viau, P. Toneguzzo, A. Pierrard, O. Acher, F. Fievet-Vincent, F. Fievet, Scr. Mater. 44 (2001) 2263.
[25] Y. Tian, J.H. Fendler, Chem. Mater. 8 (1996) 468.
[26] Y.P. Fang, A.W. Xu, L.P. You, R.Q. Song, J.C. Yu, H.X. Zhang, Q. Li, H.Q. Liu, Adv. Funct. Mater. 13 (2003) 955–960.
[27] X. Wang, Y. Li, Chem. Eur. J. 9 (2003) 5627–5635.
[28] J.B. Langford, Aust. J. Phys. 41 (1988) 173–187.
[29] B.G. Hyde, L. Eyring, Rare Earth Science Research III, Science Publishers Inc., New York, 1965, p. 289.
[30] J. Zhang, R.B. Von Dreele, L. Eyring, J. Solid State Chem. 104 (1993) 21–32.
[31] B.R. Judd, Phys. Rev. 127 (1962) 750.
[32] B. Mercier, C. Dujardin, G. Ledoux, C. Louis, O. Tillement, P. Perriat, J. Appl. Phys. 96–1 (2004) 650–653.
[33] G. Ledoux, B. Mercier, C. Louis, C. Dujardin, O. Tillement, P. Perriat, Radiat. Meas. 38 (2004) 763–766.
[34] M. Fox, Optical Properties of Solids, Oxford University Press, Oxford, 2001.
[35] A. Huignard, V. Buissette, G. Laurent, T. Gacoin, J.P. Boilot, Chem. Mater. 14 (2002) 2264–2269.